# Thermal-optical design of a geodetic satellite for one millimeter accuracy

**David A. Arnold**
Smithsonian Astrophysical Observatory, Cambridge, MA, U.S.A. (retired)

**Abstract:**

The LAGEOS (LAser GEOdynamic Satellite) satellites use a 1.5 inch uncoated retroreflector (cube corner). Design studies done for LAGEOS-1 showed that using smaller cubes would result in greater accuracy and lower thermal gradients. However, this would require using a larger number of cubes. Simulations showed that the accuracy goal of 5 millimeters could be met using 1.5 inch cubes by adding a dihedral angle offset. The LARES (LAser RElativity Satellite) satellite launched in 2012 is a smaller version of LAGEOS using the same size cube corner and floating mount as LAGEOS.

The recent development of COTS (Commercial Off-The-Shelf) cube corners has eliminated cost as an obstacle to using a larger number of smaller cubes. COTS cubes have no dihedral angle offset. However, no offset is needed if the size is chosen properly. The diffraction pattern of a 1.0 inch uncoated cube with no dihedral angle offset has 6 lobes around the central peak due to total internal reflection, The velocity aberration for LAGEOS is about 32 to 40 microradians. The OCS (Optical Cross Section) of a one inch uncoated COTS retroreflector is about .5 million sq m for the LAGEOS orbit.

Testing of 10 inexpensive COTS cubes by Ludwig Grunwaldt and Reinhart Neubert shows good cross section (unpublished work done at GFZ Potsdam, Germany). Measurement of 50 COTS cubes at INFN (Mondaini, C., et al., 2018), shows a loss of cross section of only 33 % (Slide 10). Simulations show that systematic range errors on the order of a half millimeter are possible for a spherical geodetic satellite such as LARES. Adjustments for the holding and ejection system result in some loss of accuracy.

**Keywords**: LAGEOS; retroreflectors; COTS cubes; laser ranging.
David A. Arnold
david-arnold@earthlink.net.

Contents:

## 1. Introduction and definition of terms.

The data from earth observation satellites is put into the International Terrestrial Reference Frame (ITRF). The ITRF is maintained by observation of a set of spherical geodetic satellites with a high mass to area ratio to reduce non-gravitational forces. The spherical shape simplifies calculation of the perturbations and makes the observations independent of the orientation of the satellite. The most accurate of these satellites are LAGEOS (Fig. 1.),

Fig. 1. LAGEOS.

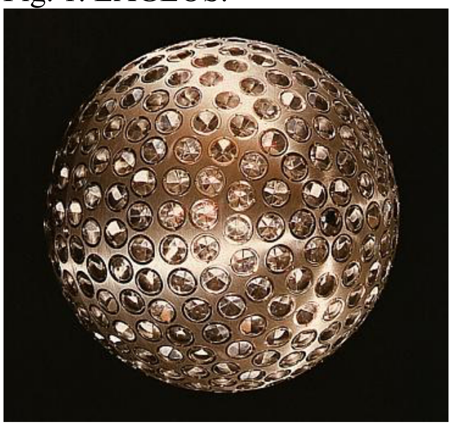

and LARES (Fig. 2.1).

Fig. 2.1 LARES.

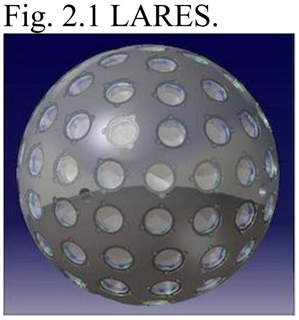

LAGEOS-1 was launched in 1976. LAGEOS-2, launched in 1992, is an exact copy of LAGEOS-1. LARES, a smaller version of LAGEOS, was launched in 2012.

The accuracy goals of the earth observation satellites are continually increasing. The current goal is one millimeter. No geodetic satellite currently in orbit can provide this accuracy. This paper develops a method of building a geodetic satellite that can provide one millimeter accuracy.

Geodetic satellites are tracked by timing short laser pulses reflected from the cube corners on the satellite. The sections below define specialized terms commonly used in satellite laser ranging. All calculations in this paper are done for wavelength 532 nanometers.

### 1.1 Velocity aberration.

In the inertial coordinate system of a retroreflector, a beam of light entering the retroreflector will be returned along the same line that it entered. If there is a difference in velocity between the retroreflector and the transmitter, the beam will not be returned to the source because the source has moved. The usual situation is that the retroreflector is in orbit and the transmitter is on the ground. We will consider the retroreflector to be stationary and the transmitter to be moving. The geometry is shown in Fig. 2.2.

Fig. 2.2. Velocity aberration.

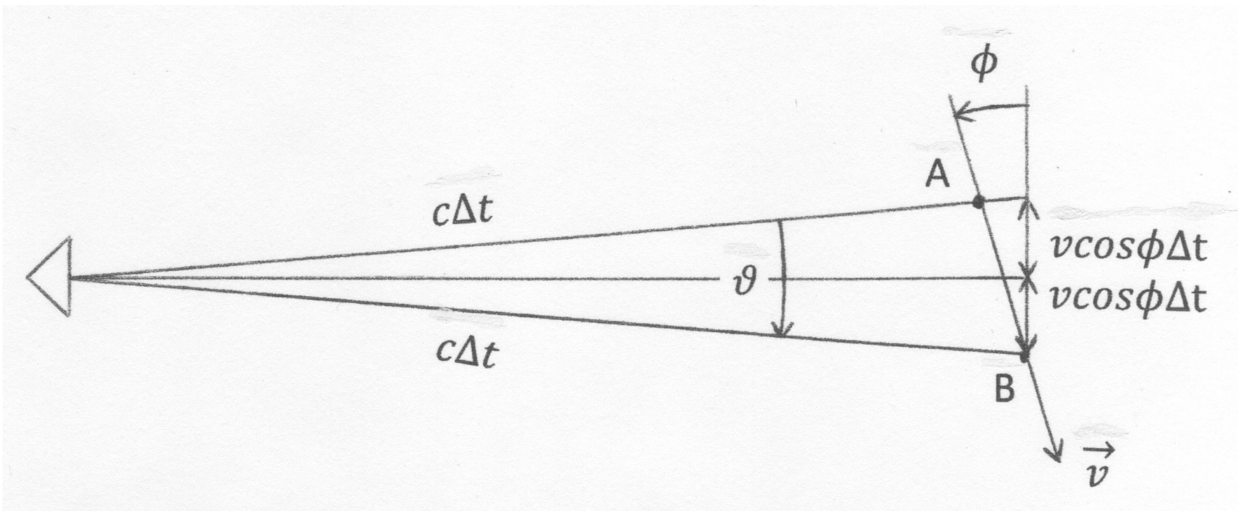


A transmitter emits a pulse of light at point A which travels in time $\Delta t$ at velocity $c$ to a retroreflector. The center of the reflected beam returns to point A after another time interval $\Delta t$. In time $2\Delta t$, the transmitter moving at velocity $v$ at an angle $\phi$ from a line perpendicular to the line of sight moves to point B. In order for the transmitter to receive any of the reflected light at point B, the angular radius $\vartheta$ of the reflected beam must be at least

$$\vartheta = \frac{2v\cos\phi\Delta t}{c\Delta t} = 2\frac{v}{c}\cos\phi$$

where $\vartheta$ is the velocity aberration.

### 1.2 Range correction and centroid.

The reflection from a spherical satellite will have pulses from each of the active retroreflectors on the side of the satellite facing the incident beam. The range to each cube corner is different. This creates a complicated return pulse. In this paper, the position of the return pulse will be defined as the centroid, i.e., the weighted mean position of the reflections from all the active reflectors. The difference between the range to the center of the satellite and the range measured to the retroreflectors is defined as the range correction. The range correction is added to the range measured to the retroreflectors on the surface of the satellite.

**1.3 Diffraction, FFDP (Far Field Diffraction Pattern), and OCS (Optical Cross Section).**

The reflections from the retroreflectors will initially be narrow, collimated beams of light. However, by the time the reflections reach the receiver they will have spread and overlapped due to diffraction. The diffraction pattern of each retroreflector will be different since they are at different incidence angles. The position of the receiver in the diffraction pattern will be determined by the magnitude and direction of the relative velocity between the transmitter and the retroreflector (see Section 1.1). The strength of the signal at the receiver will depend on the intensity of the diffraction pattern at the position of the receiver.

For convenience in computing signal strength, the term cross section has been defined. See Eq. (16) in Section 10. It is proportional to the intensity of the diffraction pattern but is given in units of area, typically million square meters. One can think of the cross section of a retroreflector array as proportional to the area of a diffuse reflecting surface in space that gives the same signal as the retroreflector array at a particular point in the far field. The cross section and range correction are different at each point in the far field and are given as matrices.

The analysis in this paper consists primarily of computing and analyzing the far field centroid and cross section matrices for a retroreflector array.

**1.4 Centroid range correction matrix, and cross section matrix.**

The range correction and cross section are computed as square matrices large enough to cover the maximum velocity aberration (see Section 1.1). The center of the matrix is at point A where the laser signal was transmitted in the inertial coordinate system of the retroreflector. The range correction and cross section will depend on the position of the receiver at point B in the far field.

I developed software for computing the far field range correction and cross section matrices as part of the design studies for LAGEOS-1 during the early 1970s. This software was needed to accurately account for diffraction.

To the best of my knowledge no one else has computed the far field centroid and cross section matrices for a retroreflector array. I don't know of any papers on this subject by other investigators.

**2. Perturbations to the diffraction pattern.**

For a perfect reflector, the exiting wavefront is flat with constant phase across the aperture. The far field pattern for a circular aperture is the well-known Airy pattern (Section 10). The radius of the central peak of the Airy pattern is $1.22\lambda/D$ where $\lambda$ is the wavelength and $D$ the diameter of the cube corner. In this paper all simulations are done at wavelength 532 nanometers.

In a solid cube corner, there are various physical effects that alter the phase and amplitude of a ray as it passes through the cube corner:

1. Phase changes due to total internal reflection for uncoated cubes.
2. Dihedral angle offsets.
3. Changes in index of refraction due to thermal gradients.
4. Variations in index of refraction of the material
5. Surface roughness
6. Darkening of the material due to radiation damage in space.
7. Reflection losses at the back faces if the cube corner is coated.
8. Fresnel reflection losses on entering and leaving the front face.

There should be no problem with radiation in COTS or custom-made cubes made from fused silica. Radiation damage to fused silica and quartz is discussed in "Induced optical absorption in gamma, neutron and ultraviolet irradiated fused quartz and silica" (Marshall, C.D., 1997). If other materials are used, they should be tested for radiation damage. Measurement of 50 COTS cubes at INFN (Mondaini, C., et al., 2018), shows a loss of cross section of only 33 % (Slide 10).

The phase changes due to total internal reflection results in 6 lobes around the central peak of the diffraction pattern. The size of the cube corner can be adjusted so that velocity aberration puts the receiver on this ring of 6 spots around the central peak (Fig. 2.3).

Fig. 2.3. Diffraction pattern of a one-inch uncoated cube.

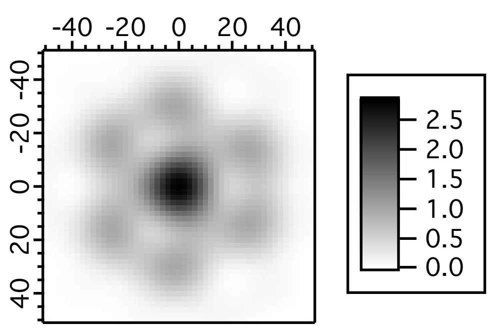


The scale of the pattern is from -50 to +50 micrordians. The cross section is in million sq m. The OCS (Optical Cross Section) of a one inch uncoated COTS retroreflector is about .5 million sq m for the LAGEOS orbit with velocity aberration 32 to 40 microradians. The clocking of the cubes in their mounting is varied to create a uniform ring around the central peak.

Dihedral angle offsets are not needed. They create a complicated diffraction pattern. In particular, the sum of the phase changes due to total internal reflection and dihedral angle offsets creates an asymmetric diffraction pattern when linear polarization is used. There will always be small dihedral angle offsets due to manufacturing errors.

The effect of thermal gradients can be minimized in a couple of ways:

1. Keep the optical path length as short as possible by using small cube corners.

2. Keep the cube corner as cold as possible to reduce thermal radiation from the front face. The LAGEOS uncoated cube corners are thermally decoupled from the core by using a floating mount to reduce conduction, and low emissivity of the mounting cavity to reduce radiative heating of the back of the cube corner.

Keeping the cube corner cold requires adjusting the thermal parameters of the core, cavity, and cube corner to minimize the temperature of the cube corner. Section 7 gives equations for doing this.

**3. Centroid vs incidence angle**

A sample array has been devised with rings of 1.0 inch uncoated cubes separated by 12 degrees on a 20.1 cm radius sphere. An analysis of this array has been done with a program that uses the equations in "Method of Calculating Retroreflector Array Transfer Functions". Smithsonian Astrophysical Observatory Special Report No. 382 (Arnold, D.A., 1978). There are 288 cubes. The array geometry is given in Table 1.

Table 1. Positions of the cube corners.

| Ring | Latitude | # of CCRs |
|---:|---:|---:|
| 1 | 90 | 1 |
| 2 | 78 | 6 |
| 3 | 66 | 12 |
| 4 | 54 | 18 |
| 5 | 42 | 22 |
| 6 | 30 | 26 |
| 7 | 18 | 29 |
| 8 | 6 | 30 |
| 9 | -6 | 30 |
| 10 | -18 | 29 |
| 11 | -30 | 26 |
| 12 | -42 | 22 |
| 13 | -54 | 18 |
| 14 | -66 | 12 |
| 15 | -78 | 6 |
| 16 | -90 | 1 |

In order to study the uniformity of the placement of the cubes, an analysis has been done with the incidence angle starting at the North pole and spiraling around the satellite down to the equator. The direction of the incidence beam is incremented by 5 degrees in Longitude between points. This goes around the satellite in 72 points. The Latitude decreases slightly between each point to make the Latitude decrease by about 5 degrees on each revolution. Because these are angular coordinates, the points are very close together at the pole (Latitude 90 deg). The distance between points increases as the Latitude decreases. The full centroid matrix is computed at each incidence angle. In order to have a single number to plot, the average centroid range correction in the velocity aberration annulus for LAGEOS (32 - 40 microradians) is computed and plotted in Fig. 3.

Fig. 3. Centroid vs Colatitude.

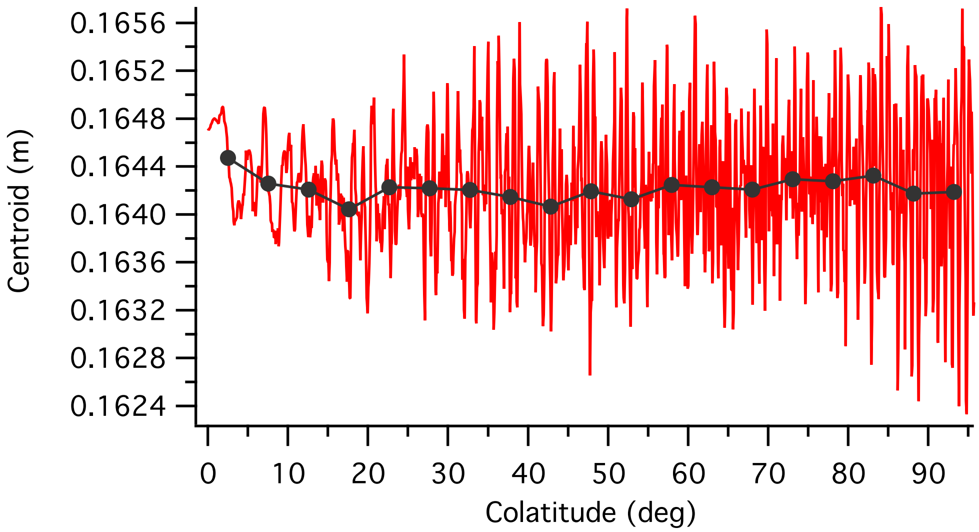


The statistical variation of the range measurements above are shown in Table 2.1 and Table 2.2.

Table 2.1. Statistics for the red line (all points).

| Minimum | Maximum | Max - Min | Average | Rms |
|---|---|---|---|---|
| 0.1623 | 0.1657 | 0.0034 | 0.1642 | 0.0006 |

Table 2.2. Statistics for the black line (average over sets of 72 points).

| Phi | minimum | Phi | maximum | max-min |
|---|---|---|---|---|
| 17.6050 | 0.1640 | 2.4850 | 0.1645 | 0.0004 |

There are peak to peak variations in centroid up to about 3 mm in range as the incidence angle changes. Since scientific analyses use a large number of range measurements the primary concern is systematic variations in centroid with Latitude. Averaging over sets of 72 points (5 deg in Latitude) shows that the systematic errors are less than the one millimeter goal for geodetic satellites.

**4. Polarization asymmetry.**

In an uncoated cube, there is an interaction between dihedral angle offsets and phase changes due to total internal reflection. This results in an asymmetrical diffraction pattern if linear polarization is used. The pattern has approximate circular symmetry for circular polarization. The asymmetry can be virtually eliminated if no dihedral angle offset is used. See Section 2B of Arnold, D.A., 2002. An offset of 1.25 arcsec in the 1.5 inch cubes is necessary to account for velocity aberration. If 1.0 inch uncoated cubes are used the diffraction pattern is wide enough to account for velocity aberration without the need for a dihedral angle offset.

Simulations have been done comparing 1.5 and 1.0 inch uncoated cubes. The first design uses 204 1.5 inch cubes on a 200 mm radius satellite. The second design uses 303 1.0 inch cubes on a 202 mm radius satellite. The range correction and cross section matrices for the satellite are irregular at a single incidence angle for both circular and linear polarization. A similar effect happens in LAGEOS (See section 4A, Arnold, D.A., 2002). The matrices have been averaged over 2520 orientations of the satellite. When this is done a nearly circular pattern appears for circular polarization. An asymmetric pattern appears for linear polarization when a dihedral angle offset is used. The same effect occurs in LAGEOS (See section 4B, Arnold, D.A., 2002). This results in a systematic range error for large data sets. The range correction is different for the two designs since the cubes and the spheres are different sizes. The scale of the figures below is -50 to +50 μrad. The far field centroid and cross section matrices have been computed and plotted.

The far field centroid matrices 4.1 and 4.2 are for a 1.5 inch cube with a 1.25 arcsecond dihedral angle offset. The units are meters. The centroid matrix with circular polarization is shown in Fig. 4.1.

Fig. 4.1. Centroid (m) with circular polarization, 1.5 inch.

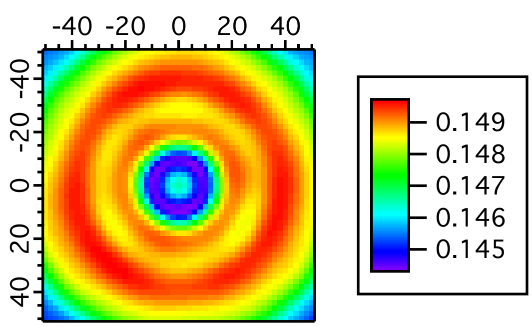


This pattern is approximately circular but there is some remaining asymmetry.

The centroid matrix with linear vertical polarization is shown in Fig. 4.2.

Fig. 4.2. Centroid (m) with linear vertical polarization, 1.5 inch.

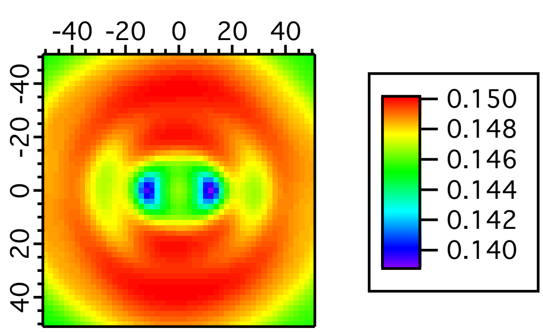

This pattern shows a well-defined asymmetry with larger centroid values aligned vertically (parallel to the linear vertical polarization). If horizontal polarization had been used the pattern would have been aligned horizontally.

The far field centroid matrices 4.3 and 4.4 are for a 1.0 inch cube with no dihedral angle offset. The centroid matrix with circular polarization is shown in Fig. 4.3.

Fig. 4.3. Centroid (m) with circular polarization, 1.0 inch.

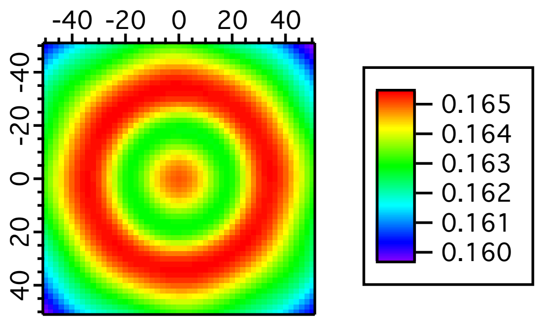


This pattern has a well-defined circular symmetry.

The centroid matrix with linear vertical polarization is shown in Fig. 4.4.

Fig. 4.4. Centroid (m) with linear vertical polarization, 1.0 inch.

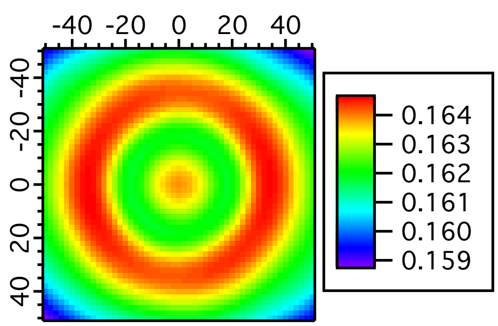


As a result of eliminating the dihedral angle offset this pattern is nearly circular despite the use of linear polarization. There is a very small remaining asymmetry that shows up only when looking at the numerical data. Circular polarization produces an approximately circular pattern for both size cubes.

The next four far field patterns are the cross section matrices corresponding to the four centroid patterns shown above. The cross section matrices 4.5 and 4.6 are for a 1.5 inch cube with a 1.25 arcsecond dihedral angle offset. The cross section matrices 4.7 and 4.8 are for a 1.0 inch cube. The units are million sq meters. The plot is inverted gray scale where dark values represent higher cross section. The cross section matrix for a 1.5 inch cube with circular polarization is shown in Fig. 4.5.

Fig. 4.5. Cross section (million sq m) with circular polarization, 1.5 inch.

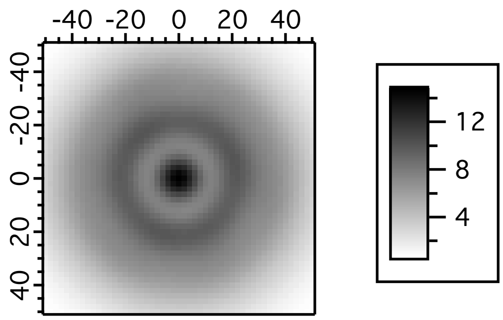


The pattern has good circular symmetry

The cross section matrix with linear vertical polarization is shown in Fig. 4.6.

Fig. 4.6. Cross section (million sq m) with linear vertical polarization, 1.5 inch.

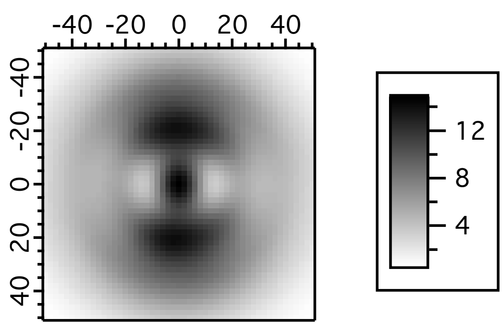


The pattern has a "dumbel" shape with bright spots aligned vertically. If horizontal linear polarization had been used the spots would have been aligned horizontally.

The far field cross section matrices 4.7 and 4.8 are for a 1.0 inch cube with no dihedral angle offset. The cross section matrix for a 1.0 inch cube with circular polarization is shown in Fig. 4.7.

Fig. 4.7. Cross section (million sq m) with circular polarization, 1.0 inch.

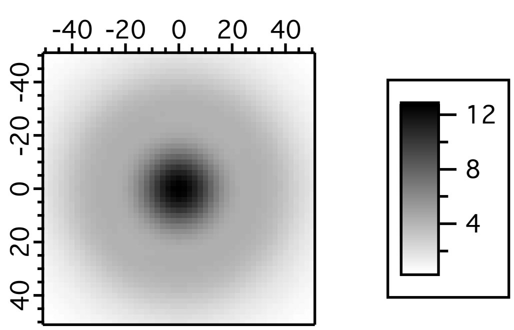


The pattern has good circular symmetry.

The cross section matrix for a 1.0 inch cube with linear vertical polarization is shown in Fig. 4.8.

Fig. 4.8. Cross section (million sq m) with linear vertical polarization, 1.0 inch.

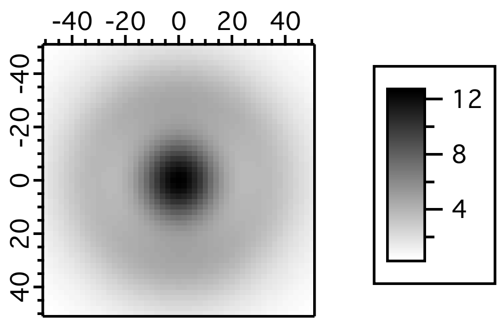


The pattern has good circular symmetry since there is no dihedral angle offset.

The maximum and minimum values of the centroid have been computed around circles of increasing radius in the far field. The asymmetry has been computed as the maximum minus the minimum. This difference has been plotted vs the magnitude of the velocity aberration. A comparison of the asymmetry for three of the cases above is plotted in Fig. 4.9.

Fig. 4.9. Asymmetry vs velocity aberration

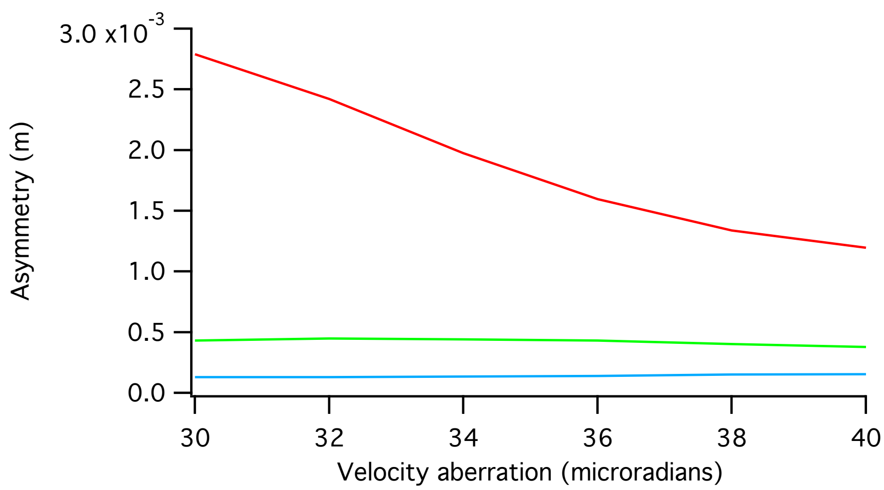


The red line (top) is for the 1.5 inch cube with a 1.25 arcsecond dihedral angle offset and linear polarization. The green line (middle) is for a 1.0 inch cube with linear polarization and no dihedral angle offset. The blue line (bottom) is for a 1.0 inch cube with circular polarization and no dihedral angle offset.

With the 1.0 inch cubes and no dihedral angle offset the asymmetry is less than .5 mm.

**5. Centroid vs velocity aberration.**

This section computes the dependence of the centroid on velocity aberration for a 1.5 inch cube and a 1.0 inch cube. Using a 1.0 inch cube places the velocity aberration on the 6 spots around the central peak. This minimizes the variation in cross section over the velocity aberration interval. Keeping the cross section more constant also reduces the variation in centroid. The velocity aberration varies from about 32 and 40 microradians at the LAGEOS altitude. Linear vertical polarization is used since this is the worst case. The variation of the centroid around circles of increasing radius in the far field has been computed. The average, maximum, and minimum around the circles has been computed at each point. The results for a 1.5 inch cube are plotted in Fig. 5.1.

Fig. 5.1. Centroid vs velocity aberration for a 1. 5 inch cube with linear polarization.

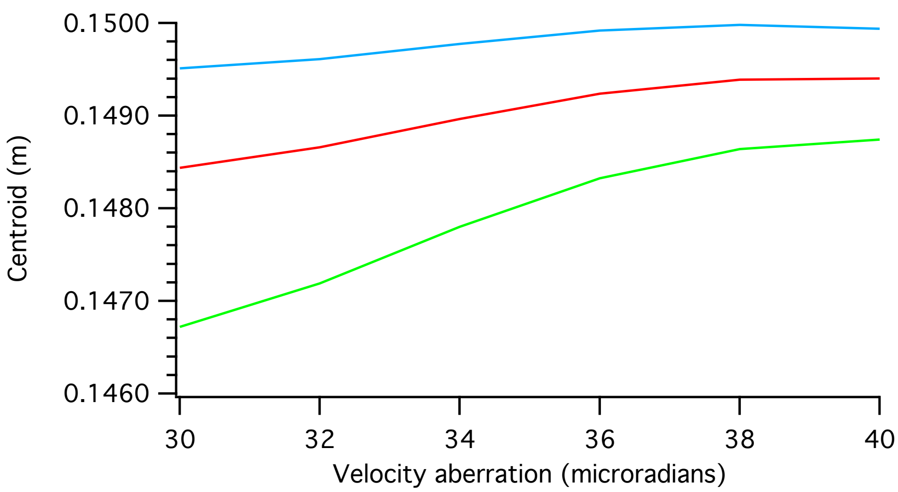


The red line (middle) is the average centroid around a circle in the far field. The green line (bottom) is the minimum. The blue line (top) is the maximum.

The average (red curve) for the 1.5 inch cube changes by .74 mm from 32 to 40 microradians. However, the asymmetry of the pattern can cause changes in centroid up to almost 3 mm depending on the direction of the velocity aberration.

The same analysis has been done for a 1.0 inch uncoated cube with no dihedral angle offset. The results are plotted in Fig. 5.2

Fig. 5.2. Centroid vs velocity aberration for a 1.0 inch cube with linear polarization.

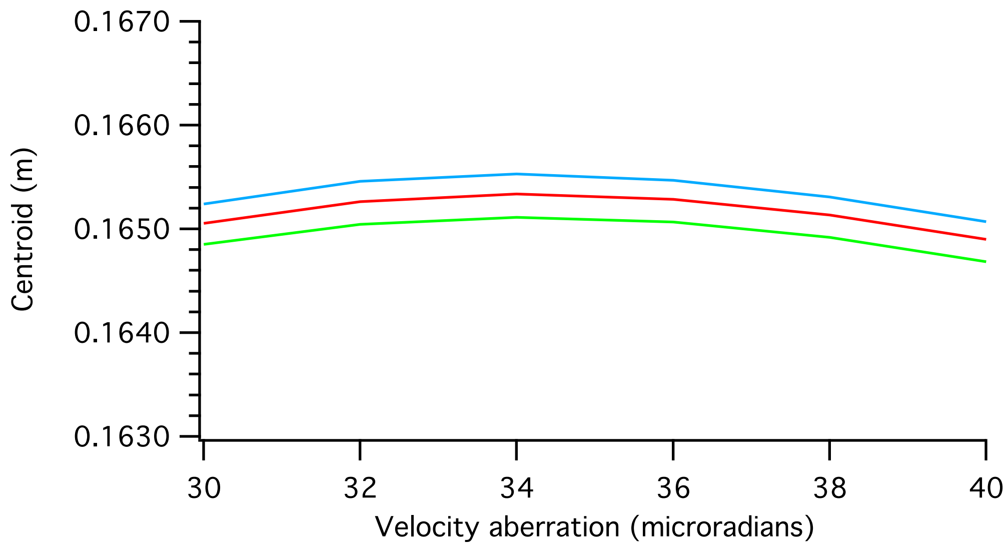


The red line (middle) is the average centroid around a circle in the far field. The green line (bottom) is the minimum. The blue line (top) is the maximum.

The change of the red curve is .47 mm for the 1.0 inch cube with very little asymmetry. This is within the accuracy goal of one millimeter. In principle, a correction could be applied as a function of velocity aberration.

**6. Thermal simulations with comparison to isothermal case**

If there were no thermal gradients the range correction would be constant. It could be measured in the lab before launch. It could be computed theoretically using the parameters of the cube corners and the measured dihedral angle offsets.

The average cross section vs velocity aberration is the same for either a positive or negative dihedral angle offset if there are no thermal gradients. As a measure of the effect of thermal gradients the cross section vs velocity aberration has been computed for a positive and a negative dihedral angle offset under various thermal conditions.

A number of thermal simulations have been done under different conditions for a 1.0 inch circular uncoated cube. Four of those simulations have been selected as representing particularly interesting conditions.

The analysis is done in four stages by programs Thermal2, Raytrace, Difract, and various analysis programs that compute the cross section and range correction around circles of increasing radius in the far field.

Program Thermal2 is a model of a retroreflector mounted in a cavity using retaining rings. It includes models for volumetric absorption of solar radiation by the cube corner, absorption of solar radiation by the reflecting surfaces of the cube corner (if metal coated), absorption of earth infrared radiation by the front face, radiative heating of the cube by the cavity and retaining rings, and conductive heating of the cube by the retaining rings.

A floating mount is simulated by setting the conductive heating of the cube corner by the mounting rings to zero. The temperature of the cavity is assumed to be constant. The retaining rings are assumed to be close to the temperature of the cavity. The cube corner is initialized to a constant temperature. The integration is continued until equilibrium is reached. The integration provides the time constants for the cube corner to reach a steady state temperature gradient. This occurs fairly rapidly. Bulk changes in cube temperature can be very slow if the thermal inputs are only radiative. The changes are more rapid if conduction is present through the mounting rings.

The output of the thermal simulations by program Thermal2 is a three-dimensional matrix giving the temperature distribution in the cube. The next step is to do a ray tracing with program Raytrace to get the phase front due to the thermal gradients. The next step is to add phase changes due to dihedral angle offsets (if any) and total internal reflection. The far field pattern is computed from the phase front by program Difract. The far field pattern is processed to compute the average cross section vs velocity aberration.

Three simulations have been run for each case. The reference case is with a dihedral angle offset of either + or - 1.25 arcsec with no thermal gradient. This is compared to the cross section vs velocity aberration with a +(>90 deg) and -(<90 deg) dihedral angle offset and thermal gradients. The phase front due to a thermal gradient may be either primarily concave or primarily convex. The phase front for a dihedral angle offset is either concave or convex depending on the sign of the dihedral angle offset. A dihedral angle offset can either add to the effect of a thermal gradient or partially cancel it.

In the four cases below, the average cross section around circles of constant velocity aberration is plotted vs the magnitude of the velocity aberration for the cube corner. For each case, the fractional change in cross section has been computed at 32 microradians.

For coated cubes there is significant absorption of solar radiation that the back metal reflecting faces. For uncoated cubes there is only the volumetric absorption which is much smaller. At the Lageos orbit height, the effect of earth infrared is lower. For simplicity, the four simulations do not include solar heating and infrared radiation from the earth. In effect, the cube is facing outer space. The dominant thermal effect is the radiation from the front face of the cube corner and the radiative heating from the mounting cavity and retaining rings. Since the radiation from the front face it proportional to the fourth power of the temperature, the thermal radiation decreases significantly with temperature. An emissivity of .9 is used for the quartz and the retaining rings.

The results for case 11 are shown in Fig. 6.1.

Fig. 6.1. Case 11, Cube 250 deg K, Core 303 deg K, floating mount

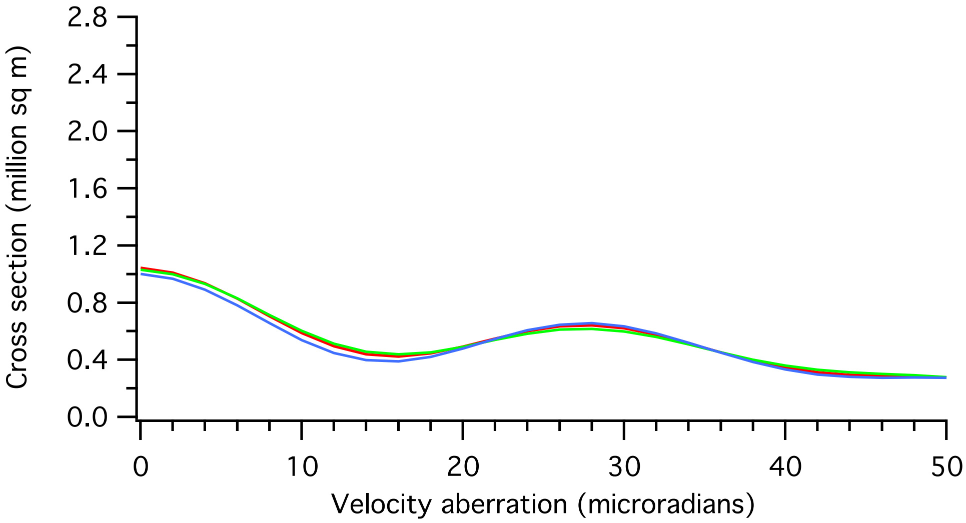


This case uses a floating mount. The cube temperature is 250 deg K. The core temperature is 303 deg K. The emissivity of the cavity is .07. The red curve (middle) is for the isothermal case with a dihedral angle offset of either + or - 1.25 arcseconds. The average cross section vs velocity aberration is the same for both. The green curve (upper) is for a -1.25 dihedral angle offset and the thermal gradient. The blue curve (lower) is for a +1.25 dihedral angle offset and the thermal gradient. The changes are so small that the curves overlap. The difference (diff) in cross section between the blue and green curves is computed at 32 microradians. The fractional change is computed as the difference (diff) divided by the largest cross section. The computation is shown in Table 3.

Table 3. Fractional change in cross section.

| microrad | -1.25 | +1.25 | diff | fraction |
|---|---|---|---|---|
| 32 | 0.55985671 | 0.58590446 | .02604 | .0444 |

This case gives the lowest thermal perturbation to the cross section. The combination of a floating mount, low cavity emissivity, and low cavity temperature results in a low cube temperature.

The results for case 12 are shown in Fig. 6.2.

Fig. 6.2. Case 12, Cube 293 deg K, Core 303 deg K, with conduction.

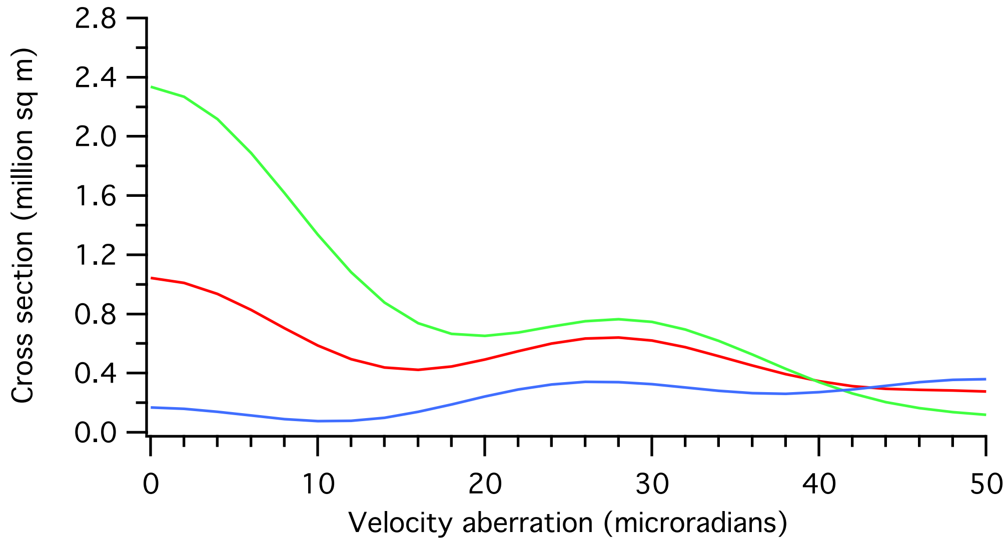


The mount conduction is .02 watts/deg K. The cube temperature is 293 K. The core temperature is 303 deg. K. The cavity emissivity is e=.07. The red curve (middle) is for the isothermal case with a dihedral angle of either + or - 1.25 arcseconds. The green curve (upper) is with a dihedral angle offset of -1.25 arcseconds and a thermal gradient. The blue curve (lower) is with a +1.25 dihedral angle offset and a thermal gradient.

The fractional change in cross section is computed using the same method as case 11. The fractional change is shown in Table 4.

Table 4. Fractional change in cross section.

| microrad | -1.25 | +1.25 | diff | fraction |
|---|---|---|---|---|
| 32 | 0.69658931 | 0.30281921 | .3937 | .5653 |

In this case the conduction through the mount raises the cube temperature significantly. There is a large perturbation to the cross section.

The results for case 16 are shown in Fig. 6.3

Fig. 6.3. Case 16, Cube 359 deg K, Core 413 deg K, high emissivity.

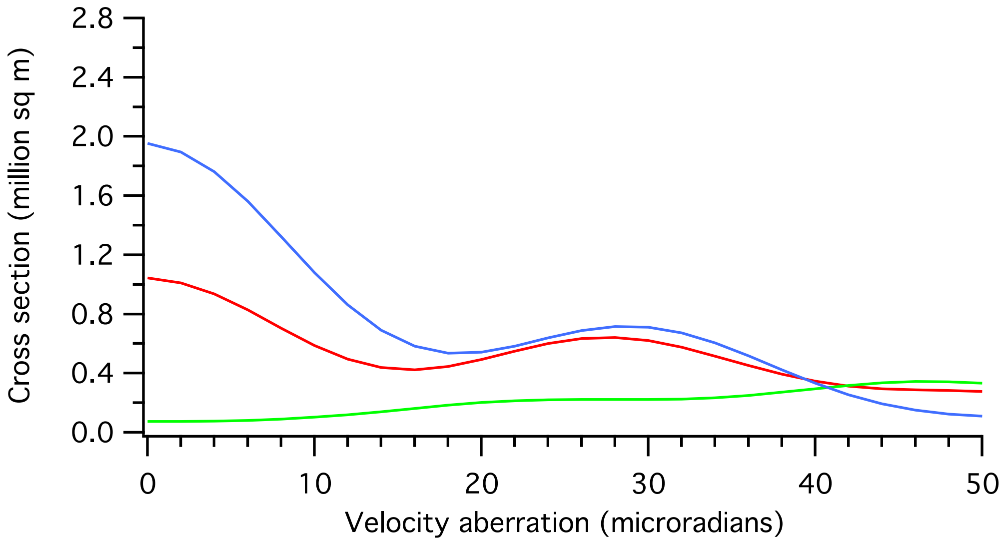


This case uses a floating mount. The cube temperature is 359 deg K. The core temperature is 413 deg K. This is a very high core temperature. The emissivity of the mounting cavity is e=.29. This is a much higher emissivity that causes more heating of the cube corner. The red curve (middle) is with dihedral angle 1.25 arcseconds with no thermal gradient. The green (lower) curve is with dihedral angle offset -1.25 arcseconds and a thermal gradient. The blue curve (upper) is with a +1.25 dihedral angle offset and a thermal gradient.

The fractional change in cross section is computed using the same method as case 11. The fractional change is shown in Table 5.

Table 5. Fractional change in cross section.

| Microrad | -1.25 | +1.25 | Diff | Fraction |
|---|---|---|---|---|
| 32 | 0.22607794 | 0.67228200 | .4462 | .6637 |

In this case the core temperature is higher, and the emissivity of the core is also higher. This produces a high cube temperature that results in large thermal perturbations.

The results of the analysis of case 17 are shown in Fig. 6.4

Fig. 6.4. Case 17. Cube 298 deg K, Core 343 deg K, high emissivity

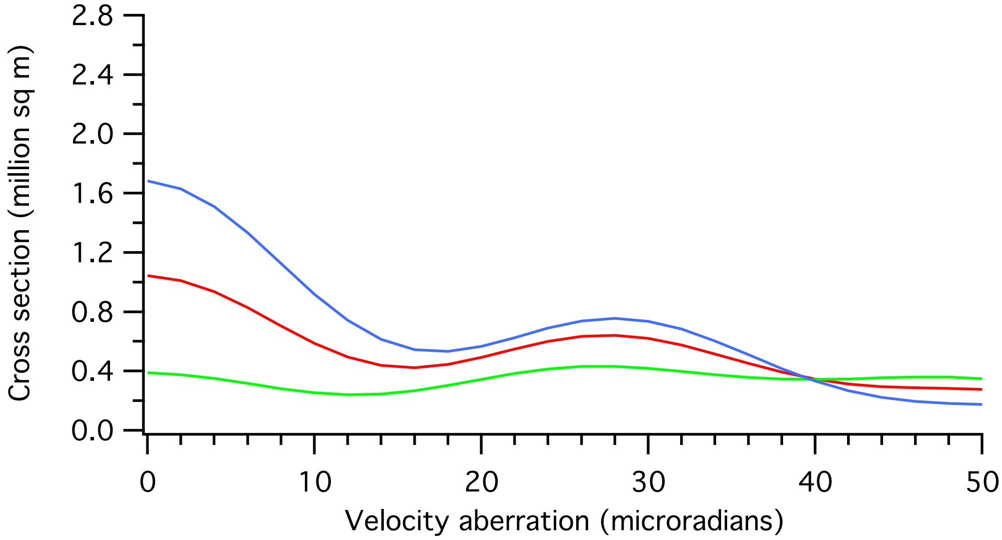


This case uses a floating mount. The cube temperature is 298 deg K. The core temperature is 343 deg K. This is lower than in case 16, but still high. The emissivity is e=.29. This gives more heating to the cube. The red curve (middle) is with dihedral angle 1.25 arcseconds with no thermal gradient. The green (lower) curve is with dihedral angle offset -1.25 arcseconds and a thermal gradient. The blue curve (upper) is with a +1.25 dihedral angle offset and a thermal gradient.

The fractional change in cross section is computed using the same method as case 11. The fractional change is shown in Table 6.

Table 6. Fractional change in cross section.

| Microrad | -1.25 | +1.25 | Diff | Fraction |
|---|---|---|---|---|
| 32 | 0.39935082 | 0.68346629 | .2841 | .4156 |

The core temperature is lower than in case 16, but the emissivity of the core is still high. The thermal perturbation is reduced somewhat compared to case 16.

The temperature of the cube and the heat conducted through the mount are the primary factors in determining the change in cross section due to thermal effects. The fractional change in cross section is plotted vs temperature in Fig. 7.1.

Fig. 7.1. Fractional change in cross section vs temperature.

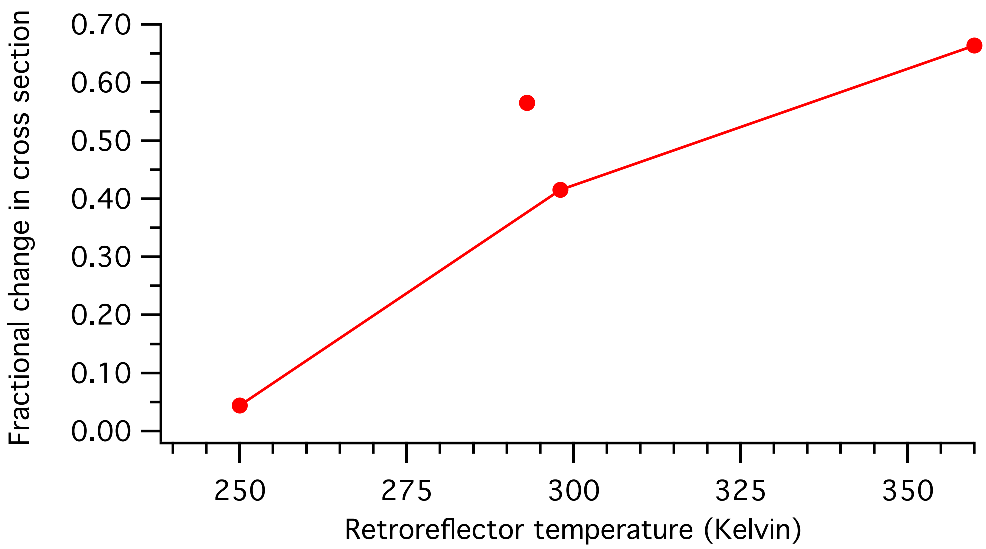


Cases 11, 17, and 16 that use a floating mount are connected by a line. The fractional change increases with temperature. Case 12 is plotted separately since there is also conduction. The mount conduction increases the change in cross section at the same cube temperature. Cases with conduction fall on a higher line than cases with a floating mount.

The data for the four thermal cases 11,12,16, and 17 are shown in Table 7.

Table 7. Data for the four thermal cases.

| Case | Core temperature | Reflector Temperature | Fractional change in cross section |
|---|---|---|---|
| 11 radiation only | 303 | 250 | .0444 |
| 17 radiation only | 343 | 298 | .4156 |
| 16 radiation only | 413 | 360 | .6637 |
| | | | |
| 12 conduction + radiation | 303 | 293 | .5653 |

The cases with radiation only (no conduction) are listed in order of the retroreflector temperature.

The data can also be plotted with the variables reversed. The temperature as a function of the fractional change in cross section is plotted in Fig. 7.2.

Fig. 7.2. Temperatures vs fractional change in cross section

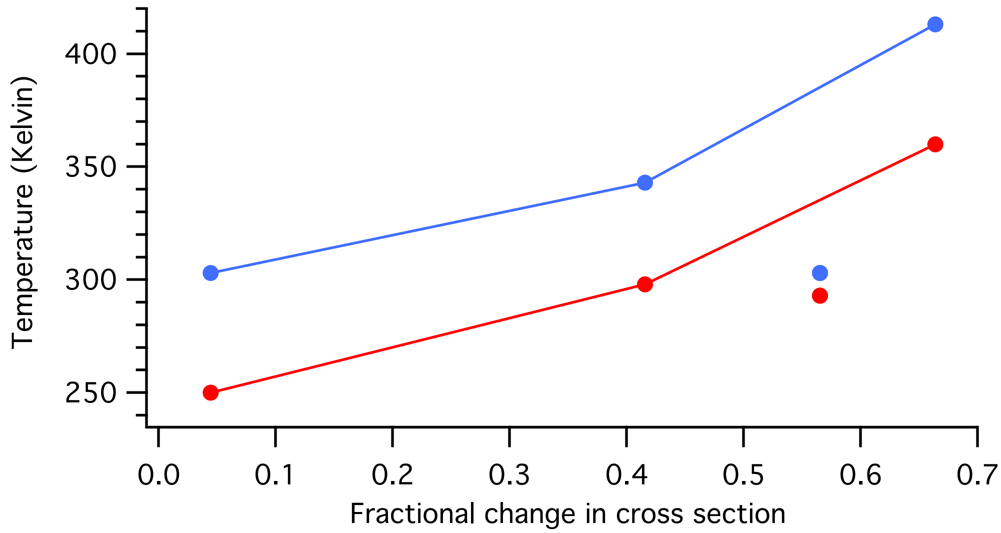


The red curve (lower) is the cube temperature. The blue curve (upper) is the core temperature. Case 12 with conduction is plotted separately as dots. The cube corner has a very high emissivity. Heat is being radiated (and conducted in case 12) from the core to the cube corner. It is then radiated from the front face of the cube corner. The core temperature is always higher than the cube temperature.

For case 12 (dots), the cube temperature (lower red dot) is almost as high as the core temperature (upper blue dot). The fractional change in cross section is high even though the core temperature is not excessively high. The heat conducted through the mount increases the temperature of the cube and also changes the temperature distribution in the cube corner. Both effects cause changes in cross section.

The temperature of the cube in case 12 with conduction depends on the conductance of the mount. The dependence of the temperature on mount conductance is plotted in Fig. 8.

Fig. 8. Retroreflector temperature vs mount conductance

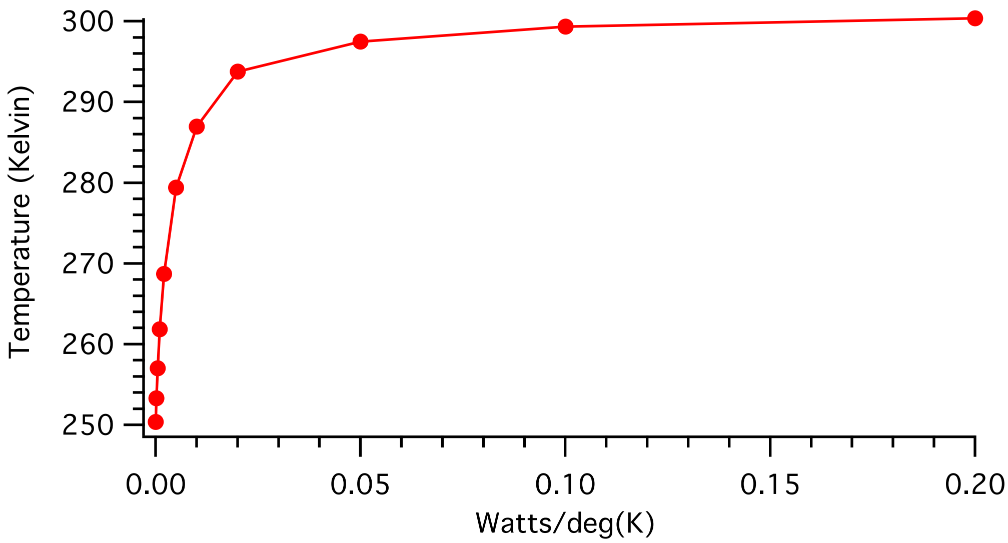


The mount conductance is in watts/deg(K). The temperature vs mount conductance is listed in Table 8.

Table 8. Cube temperature vs mount conductance.

| Mount conductance watts/deg K | Cube temperature K |
|---|---|
| .0000 | 250.38 |
| .0002 | 253.31 |
| .0005 | 257.00 |
| .0010 | 261.87 |
| .0020 | 268.69 |
| .0050 | 279.40 |
| .0100 | 286.95 |
| .0200 | 293.76 |
| .0500 | 297.48 |
| .1000 | 299.36 |
| .2000 | 300.38 |

A very small amount of conductance through the mount can have a significant effect on the temperature of the retroreflector. The effect of the conductance saturates as the temperature of the cube corner approaches the temperature of the mounting rings.

High conductivity brings the cube temperature close to the core temperature. This increases the fractional change in cross section. The floating mount is essential for keeping the cube corner as cold as possible. Case 11 shows that if the floating mount is used and the temperature of the cube is below about 250 deg K there should be negligible thermal effects. In this case, the range correction in orbit is the same as the isothermal range correction which can be measured in the laboratory or computed theoretically from the system parameters.

## 7. Equations of equilibrium

The thermal simulations show that the cube corner must be kept as cool as possible in order to minimize thermal problems. The temperature of the core and the cube depends on the absorptivity and emissivity of the core, the mounting cavity, and the cube corners. These parameters need to be chosen to minimize the temperature of the cube. If the temperature variations in the core and cube corner are small, it is possible to derive an equation for the temperature of the cubes and the core as follows.

The effective emissivity $e_{12}$ between two infinite parallel plates with emissivity $e_1$ and $e_2$ is given by the equation

$$\frac{1}{e_1} + \frac{1}{e_2} - 1 = \frac{1}{e_{12}} \qquad (1)$$

The thermal radiation from the core to the cube consists of two parts. There is radiation from the retaining rings and radiation directly from the cavity. The total thermal radiation to the cube is

$$R_{core} = \sigma\left(e_{cav}A_{cav} + e_{rings}A_{rings}\right)\left(t_{core}^4 - t_{cube}^4\right)$$

where
σ = Stefan Boltzman constant = $5.6697 \times 10^{-8}$ in MKS units
$e_{cav}$ = the effective emissivity to the core
$A_{cav}$ = the area of the cube that radiates to the core
$e_{rings}$ = the effective emissivity to the rings
$A_{rings}$ = the area of the cube that radiates to the rings
$t_{core}$ = the temperature of the cavity and retaining rings
$t_{cube}$ = the temperature of the cube corner

If we define

$$e_{eff}A_b = e_{cav}A_{cav} + e_{rings}A_{rings}$$

Then we have

$$R_{core} = \sigma e_{eff}A_b\left(t_{core}^4 - t_{cube}^4\right) \qquad (2)$$

where
$e_{eff}$ = the effective emissivity between the core and the cube corner
$A_b$ = the total surface area of the back of the cube corner

This initial analysis neglects the mounting rings. Since the radiation from the rings and the cavity differs only by a constant with the same temperature dependence the rings can easily be added to the computation in the term $e_{eff}A_b$.

The temperature of the cube varies by a couple of degrees between the front and the back. Using the average temperature of the cube is adequate for computing the approximate equilibrium temperature.

The heat conducted through the mounting is

$$C_m = c(t_{core} - t_{cube}) \tag{3}$$

where $c$ is the conductance of the mount.

The thermal radiation from the front face is

$$R_f = \sigma e_{cube} A_f T_{cube}^4 \tag{4}$$

where
$e_{cube}$ = emissivity of the front face
$A_f$ = the area of the front face

The equilibrium temperature is given by

Heat emitted = heat absorbed

$$\sigma e_{cube} A_f t_{cube}^4 = R_{core} + H_{cube} \tag{5}$$

Where $H_{cube}$ is all other heating such as conduction from the core, solar radiation, and earth infrared.

Substituting Eq. (2) into Eq. (5) gives

$$\sigma e_{cube} A_f T_{cube}^4 = \sigma e_{eff} A_b (t_{core}^4 - t_{cube}^4) + H_{cube} \tag{6}$$

Combining terms we have

$$\left(\sigma e_{eff} A_b + \sigma e_{cube} A_f\right) t_{cube}^4 = \sigma e_{eff} A_b t_{core}^4 + H_{cube} \tag{7}$$

The equilibrium temperature is given by

$$t_{cube}^4 = \frac{\sigma e_{eff} A_b t_{core}^4 + H_{cube}}{\sigma e_{eff} A_b + \sigma e_{cube} A_f} \tag{8}$$

The heat inputs and outputs to the core are:

1. Thermal radiation to the cube.
2. Heat conducted to the cube through the mount.

3. Thermal radiation from the surface not covered by cube corners.
4. Solar radiation.
5. Earth infrared radiation.

Eq. (6) gives the thermal balance for the cube. It gives a relationship between the temperature of the core and the cube. The thermal balance equation for the core is

Heat emitted = heat absorbed

$$\sigma e_{core} A_{core} t_{core}^4 + N R_{core} = H_{core} \quad (9)$$

N is the number of cubes and $H_{core}$ is all other heat transfer such as energy received from solar radiation and earth infrared, and energy transferred to the cube by conduction.

Substituting Eq. (2) into Eq. (9)

$$\sigma e_{core} A_{core} t_{core}^4 + N\sigma e_{eff} A_b (t_{core}^4 - t_{cube}^4) = H_{core} \quad (10)$$

Combining terms,

$$\left(\sigma e_{core} A_{core} + N\sigma e_{eff} A_b\right) t_{core}^4 = N\sigma e_{eff} A_b t_{cube}^4 + H_{core} \quad (11)$$

Eq. (11) is the thermal balance equation for the core. It contains the temperature of the core and the temperature of the cube. Eq. (8) can be used to eliminate the temperature of the cube.

Substituting Eq. (8) into Eq. (11) gives

$$\left(\sigma e_{core} A_{core} + N\sigma e_{eff} A_b\right) t_{core}^4 = N\sigma e_{eff} A_b \frac{\sigma e_{eff} A_b t_{core}^4 + H_{cube}}{\sigma e_{eff} A_b + \sigma e_{cube} A_f} + H_{core} \quad (12)$$

Eq. (12) contains only the temperature of the core. This equation can be solved for the temperature of the core as a function of the physical constants. Combining terms gives

$$\left[\sigma e_{core} A_{core} + N\sigma e_{eff} A_b \left(1 - \frac{\sigma e_{eff} A_b}{\sigma e_{eff} A_b + \sigma e_{cube} A_f}\right)\right] t_{core}^4 = N\sigma e_{eff} A_b \frac{H_{cube}}{\sigma e_{eff} A_b + \sigma e_{cube} A_f} + H_{core} \quad (13)$$

Cancelling and combining factors of σ gives

$$\sigma \left[e_{core} A_{core} + N e_{eff} A_b \left(1 - \frac{e_{eff} A_b}{e_{eff} A_b + e_{cube} A_f}\right)\right] t_{core}^4 = \frac{N e_{eff} A_b H_{cube}}{e_{eff} A_b + e_{cube} A_f} + H_{core} \quad (14)$$

Simplifying the term in ( ) on the left side we have

$$1 - \frac{e_{eff}A_b}{e_{eff}A_b + e_{cube}A_f} = \frac{e_{eff}A_b + e_{cube}A_f - e_{eff}A_b}{e_{eff}A_b + e_{cube}A_f} = \frac{e_{cube}A_f}{e_{eff}A_b + e_{cube}A_f}$$

Substituting the simplified expression and solving for the core temperature gives

$$t_{core}^4 = \frac{\frac{Ne_{eff}A_bH_{cube}}{e_{eff}A_b + e_{cube}A_f} + H_{core}}{\sigma\left[e_{core}A_{core} + Ne_{eff}A_b\left(\frac{e_{cube}A_f}{e_{eff}A_b + e_{cube}A_f}\right)\right]} \tag{15}$$

The core temperature computed from Eq. (15) can be substituted into Eq. (8) to obtain the cube temperature.

The terms $H_{cube}$ and $H_{core}$ contain the first power of the temperatures according to Eq. (3). If the conduction is zero this equation give the core temperature directly. If the conduction is not zero then an iterative solution is required. With a floating mount there should be negligible conduction between the mount and the cube in space.

## 8. Temperatures of Core and Cubes

Four cases have been computed. The only heating is solar radiation. The cubes are 1.0 inch in diameter. A volumetric solar absorption of 10% is used for the cubes. The path length in the 1.0 inch cube is shorter than in a 1.5 inch cube. The heating is the average over the whole sphere. The solar heating for a cube at normal incidence is divided by 4 to get the average solar heating. The temperatures of the core and cube corner for various values of the parameters are shown in Table 9.

Table 9. Core and cube corners temperatures computed from the equations in section 7.

| Col | 1 | 2 | 3 | 4 | 5 | 6 | 7 | 8 | 9 | 10 | 11 |
|---|---|---|---|---|---|---|---|---|---|---|---|
| Case | $\alpha_{core}$ | $\varepsilon_{core}$ | $\varepsilon_{cav}$ | $t_{sphere}$ | $t_{core}$ | $t_{cube}$ | $H_{core}$ | $H_{cube}$ | $R_{core}$ | $R_{ToCube}$ | $R_{cube}$ |
| 1 | .62 | .29 | .05 | 338.7 | 327.6 | 209.1 | 75.92 | .0177 | 66.4 | .0317 | .0494 |
| 2 | .62 | .29 | .29 | 338.7 | 302.7 | 252.5 | 75.92 | .0177 | 49.7 | .0874 | .1050 |
| 3 | .15 | .80 | .05 | 184.3 | 183.3 | 164.6 | 18.37 | .0176 | 18.4 | .0013 | .0190 |
| 4 | .15 | .80 | .29 | 184.3 | 181.0 | 170.7 | 18.37 | .0177 | 17.1 | .0043 | .0220 |

The quantities listed in the table are defined below.

Column:
1 Solar absorptivity of the core
2 Emissivity of the core
3 Emissivity of the cavity
4 Temperature of a sphere with no cube corners
5 Temperature of the core
6 Temperature of a cube

7  Solar heating of the core
8  Solar heating of a cube corner
9  Thermal radiation from the core
10 Thermal radiation to a cube corner
11 Radiation from the front face of a cube corner

The amount of heating is independent of the emissivity of the cavity. Changing the emissivity changes the ratio of the heat radiated by the core and the cubes. When the emissivity of the cavity is increased more heat is radiated by the cube corner. The temperature of the core goes down but the temperature of the cube goes up. Column 11 shows the increase in the heat passing through the cube. This is what causes the thermal gradients.

Cases 1 and 2 are for a brushed metal, such as nickel. The thermal constants of nickel from the document "Thermo-Optical Properties" by Isidoro Martinez (reference Martinez,I.), are absorptivity = .20, and emissivity .05. If nothing is done to the surface of the cavity the emissivity should be about .05. If the surface of the sphere is sand blasted or brushed this can increase the emissivity. It also increases the solar absorptivity. If the emissivity increases more than the absorptivity the net result is to cool the core.

A better approach is shown by Cases 3 and 4. These cases assume some kind of OSR (Optical Solar Reflector, or Second Surface Reflector). Metals tend to have a higher solar absorptivity and lower emissivity as seen in the case of nickel. Metals tend to run hot. Glasses have a low solar absorptivity and a high emissivity. Glasses tend to run cold. In an OSR the solar radiation passes through a thin layer of glass and is reflected from a metal surface. The metal surface absorbs some of the solar radiation. This heat is conducted to the glass and radiated from the glass. This combination achieves a very low a/e (absorptivity/emissivity) ratio.

In cases 3 and 4 the core and the cubes achieve very low temperatures.

**9. Cross section vs dihedral angle offset**

Due to manufacturing errors, there will always be some unintentional dihedral angle offset. This section shows the effect of increasing dihedral angle offset in a one-inch uncoated cube corner. The dihedral angle offset goes from 0.00 to 1.25 arcsec in 0.25 arcsec increments.

The cross section vs dihedral angle offset is shown in Fig. 9.1.

Fig. 9.1. Cross section vs dihedral angle offset.

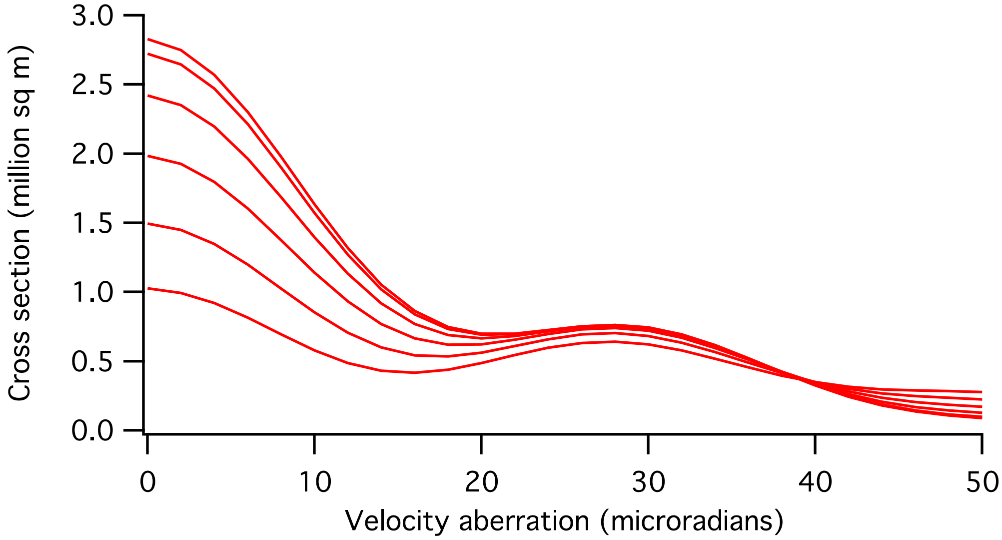


The offsets from top to bottom are 0.00, 0.25, 0.50, 0.75, 1.00, and 1.25 arcseconds. The maximum cross section is 2.829377 million sq m. In order to give better resolution in the interval between 32 and 40 microradians, the data has been replotted in Fig. 9.2.

Fig. 9.2. Expanded plot of the section between 32 and 40 microradians.

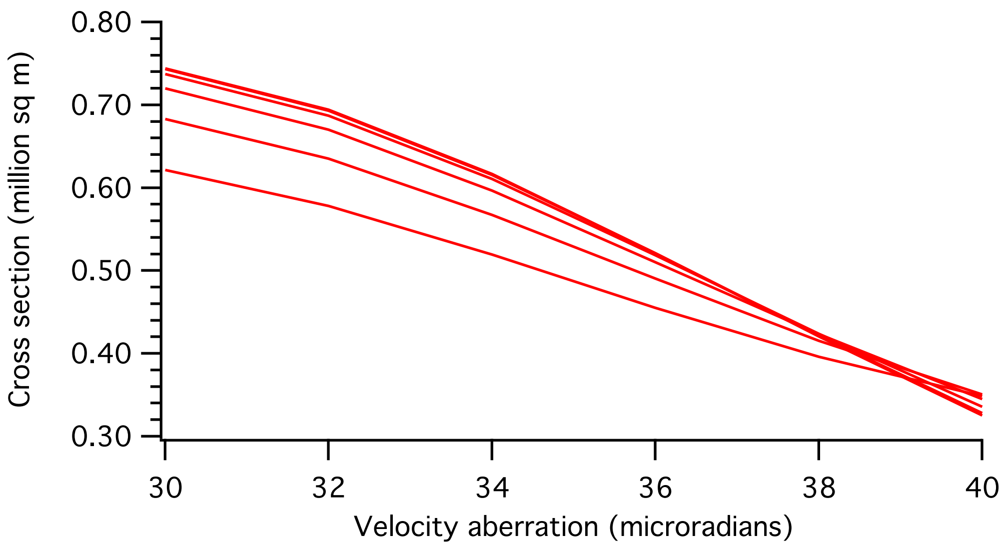


The change in the cross section with dihedral angle is quite large at the center of the pattern. However, the change at 32 microradians is only about 16 percent. The change at 39 microradians is almost zero. The stability of the cross section between 32 and 40 microradians results from placing the velocity aberration on the ring of 6 spots around the central peaks.

## 10. Airy pattern and cross section formula

The diffraction pattern of a circular aperture is the well-known Airy pattern. The cross section at the center of the Airy pattern is given by the equation

$$C = 4\pi \left(\frac{A}{\lambda}\right)^2 \tag{16}$$

Where,

$C$ = the cross section
$A$ = the area of the aperture
$\lambda$ = the wavelength

This equation is correct at the center of the diffraction pattern regardless of the shape of the aperture. It can be used to normalize diffraction patterns calculated in arbitrary units. The dependence on velocity aberration will depend on the shape of the aperture. The center of the diffraction pattern is never observed in laser ranging due to velocity aberration.

The diffraction pattern of a circular cube corner with perfect back reflecting faces is an Airy pattern. The Airy pattern is plotted in Fig. 10.1.

Fig. 10.1. The Airy pattern for a one-inch coated cube corner.

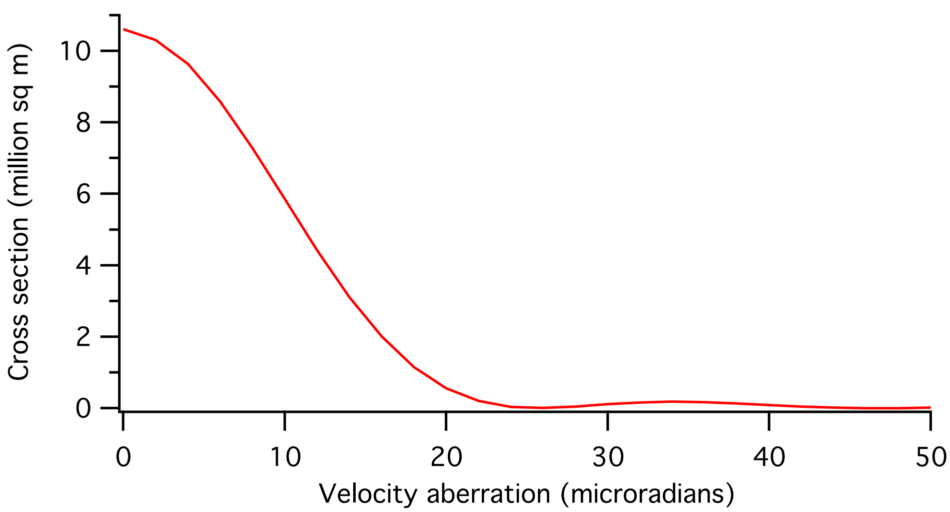


The cross section at zero microradians is 10.613809 million sq m. Using Equation (16) gives 11.39990 million sq m. The difference of a factor of 1.074 is due to reflection losses on entering and leaving the fused silica used to construct the cube corner. The cross section at the center for an uncoated cube (Section 9) is 2.829377. The ratio coated/uncoated at the center is 10.613809/2.829377 = 3.75. The Apollo Lunar cubes lost almost a factor of 4 in cross section by using uncoated cubes. This was necessary for thermal reasons. The absorption of solar radiation by the metal reflecting faces caused thermal gradients that distorted the diffraction pattern.

The intensity of the ring between 30 and 40 microradians is very week. The relative intensity is .0175 (http://hyperphysics.phy-astr.gsu.edu/hbase/phyopt/cirapp2.html#c2). The cross section on this ring could be increased by adding a dihedral angle offset. However, this would require using expensive custom made cubes.

Using an uncoated cube increases the cross section between 30 and 40 microradians for a one-inch cube corner. The difference is shown in Fig. 10.2.

Fig. 10.2. Comparison of coated and uncoated one-inch cube corner.

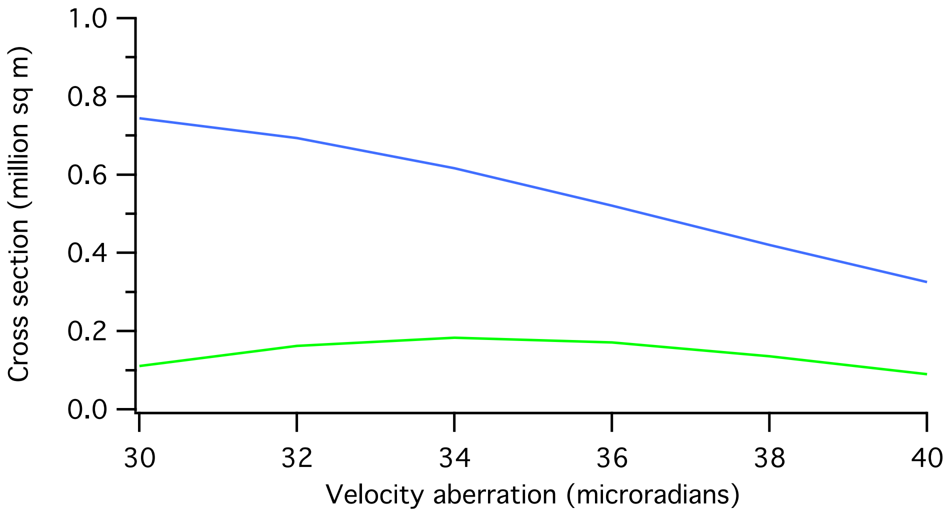


The blue curve (top) is for an uncoated cube corner.
The green curve (bottom) is for a coated one-inch cube corner.
Using uncoated cubes increases the cross section between 30 and 40 microradians without the use of a dihedral angle offset.

**11. Summary.**

The use of small cubes eliminates the need for dihedral angle offsets. This allows the use of inexpensive COTS cubes. The small cubes produce a much more accurate isothermal range correction. If the temperature of the cube is less than about 250 deg K the percent change in cross section due to thermal gradients should be negligible. In this case the isothermal range correction will be very close to the actual range correction in orbit.

The benefits of using small cubes are:

**1**. There is more uniform coverage of the surface and smaller variations with incidence angle.

**2**. The 1.5 inch cubes are too large for the velocity aberration and required dihedral angle offsets. This produces a "lumpy" diffraction pattern that causes variations in range within the far field diffraction pattern.

**3**. There is an interaction between dihedral angle offsets and the phase changes due to total internal reflection that produces an asymmetrical diffraction pattern when linear polarization is used.

**4**. The 1.0 inch cubes provide the necessary beam spread to account for velocity aberration without the need for dihedral angle offsets. This also removes the asymmetry in the diffraction pattern with linear polarization.

**5**. The diffraction pattern without dihedral angle offsets is smoother than the patterns with offsets.

**6**. The diffraction pattern of an uncoated cube has a ring of spots around the central peak. The size of the cube can be chosen to put the velocity aberration on this ring of spots rather than on a slope in the diffraction pattern. This reduces the variation of the range correction with velocity aberration. This ring of spots is a very stable part of the diffraction pattern that does not change much due to various perturbations.

**7**. The reduction in size from 1.5 to 1.0 inches appears to reduce variations in the cross section by about a factor of 5 or 6.

**8**. Eliminating the dihedral angle offset makes it possible to use COTS (Commercial Off-The-Shelf) cubes that are inexpensive and available quickly.

**9**. There are small unintentional dihedral angle offsets in COTS cubes that are generally less than one arsec but can be up to two arcsec. The effect of a positive (>90 deg) offset is in the opposite direction from the effect of a negative (<90 deg) offset. Since the mean offset is zero the positive offsets tend to partially cancel the effect of the negative offsets.

**10**. Thermal simulations show that the effect of thermal gradients in a 1.0 inch cube is very small with a floating mount and low emissivity of the mounting cavity.

**11**. A floating mount requires leaving a small gap between the ring and the cube. This could potentially result in damage to the cube due to vibrations during launch. Vibration testing should be done to determine if a particular design can withstand the vibration of launch.

**12**. The thermal simulations show that the fractional change in cross section due to thermal gradients is primarily a function of the temperature of the cube if a floating mount is used.

## 12. References.


Arnold, D.A., 1978, Method of Calculating Retroreflector Array Transfer Functions. Smithsonian Astrophysical Observatory Special Report No. 382, 165 pp. http://www.davidarnoldresearch.org/1979SAO382.pdf, or, https://ilrs.cddis.eosdis.nasa.gov/docs/1979/1979SAOSR_382.pdf

Arnold, D.A., 2002, Retroreflector Array Transfer Functions. Presentation to 13th International Workshop on Laser Ranging, Washington, DC, USA, October 7-11, 2002. https://ilrs.cddis.eosdis.nasa.gov/docs/retro_transfer_functions.pdf. Also available at http://www.davidarnoldresearch.org/Transfer.pdf

Marshall, C.D., et.al., Induced optical absorption in gamma, neutron and ultraviolet irradiated fused quartz and silica. Journal of Non-Crystalline Solids, Volume 212, Issue 1, May 1997, Pages 59-73.

Martinez, I.,1995-2018, Thermal-Optical Properties. http://webserver.dmt.upm.es/~isidoro/dat1/Thermooptical.pdf

Mondaini, C., et al., 2018, Characterization of the optical performance of COTS laser retroflectors for ASI-INFN Joint Projects. https://cddis.nasa.gov/lw21/docs/2018/presentations/Session6_Mondaini_presentation.pdf